Au nanoparticles target cancer

Nanoparticles with unique optical properties, facile surface chemistry, and appropriate size scale are generating much enthusiasm in molecular biology and medicine. Noble metal, especially Au, nanoparticles have immense potential for cancer diagnosis and therapy on account of their surface plasmon resonance (SPR) enhanced light scattering and absorption. Conjugation of Au nanoparticles to ligands specifically targeted to biomarkers on cancer cells allows molecular-specific imaging and detection of cancer. Additionally, Au nanoparticles efficiently convert the strongly absorbed light into localized heat, which can be exploited for the selective laser photothermal therapy of cancer. We discuss recent advances in the study and use of selectively targeted Au nanospheres in cancer photodiagnostics and photothermal therapy. By changing the shape or composition of Au nanoparticles, the SPR can be tuned to the near-infrared region, allowing *in vivo* imaging and photothermal therapy of cancer. The use of Au nanorods and silica-Au core-shell nanoparticles for *in vivo* cancer detection and therapy is discussed.

Prashant K. Jain[1], Ivan H. El-Sayed[2], and Mostafa A. El-Sayed[1,*]

[1]Laser Dynamics Laboratory, School of Chemistry and Biochemistry, Georgia Institute of Technology, Atlanta, GA 30332, USA

[2]Department of Otolaryngology-Head and Neck Surgery, Comprehensive Cancer Center, University of California at San Francisco, San Francisco, CA 94143, USA

**E-mail: melsayed@gatech.edu*

The past two decades have witnessed rapid advances in the ability to structure matter at the nanoscale with sufficient degree of control over the material size, shape, composition, and morphology[1]. Existing spectroscopy and microscopy tools have further facilitated the investigation, characterization, and design of nanostructures[2]. At the nanoscale, materials exhibit unique optical, electronic, and magnetic properties not seen at the bulk scale, which makes nanostructures attractive for a wide range

ISSN:1748 0132 © Elsevier Ltd 2007

of applications. The combination of these unique properties with the appropriate size scale has motivated the introduction of nanostructures into biology[3-7]. Cells and their constituent organelles lie on the sub-micron to micron size scale. Further, proteins and macromolecules found throughout the cell are on the nanometer size scale. Thus nanoparticles ranging from a few to a hundred nanometers in size become ideal as labels and probes for incorporation into biological systems[6,7]. Tunable surface chemistry further facilitates the coating, functionalization, and integration of nanoparticles with a host of biomolecular moieties[4]. This opens the door to a wide gamut of applications in molecular biology and biomedicine, such as drug[8] and gene[9] delivery, tissue engineering[6,10], protein and DNA sensing[11] and detection-based diagnostics[3,5,12,13], and biological/biomedical imaging[14-18].

Despite significant investment and research, cancer is still responsible for 25% of all deaths in developed countries[19]. Cancer is the second leading cause of death in the US, responsible for 22.7% of all deaths in 2003. Since 1950, the overall mortality rate per 100 000 has remained the same[20]. There is a pressing need for more sensitive, accurate, and cost-effective methods for detecting and treating cancer. With their unique optical, thermal, and electromagnetic properties, nanoparticle-biomaterial composites have tremendous potential in novel methods for detection, characterization, and therapy of cancer[21]. In this review, we focus on recent advances in the use of Au nanoparticles in the detection and photothermal therapy of cancer.

Noble metal nanoparticles and surface plasmon resonance

Of the different classes of organic and inorganic (metal, dielectric, and semiconductor) nanoparticles, noble metal nanoparticles have fascinated scientists since historic times because of their unique size- and shape-dependent optical properties[22-25]. While the most ancient use of colloidal Au is believed to have been in Egypt[26] by alchemists, the brilliant colors of nanosized colloidal particles of Ag, Au, and Cu were used in staining glasses[27] as far back as the 17th century and in decorative artworks as ancient as the Roman Lycurgus cup from the 4th century[28].

Today, the potential of noble metal nanoparticles is recognized to derive from the addressability of their interesting optical properties via spectroscopic and photonic techniques[29]. While Faraday[30] first attributed the bright colors to colloidal Au, Mie[22,24,31] explained the origin of the phenomenon by solving Maxwell's electromagnetic equation for the interaction of light with spherical particles in 1908 (see text box).

For a spherical nanoparticle much smaller than the wavelength of light (diameter d << λ), an electromagnetic field at a certain frequency (ν) induces a resonant, coherent oscillation of the metal free electrons across the nanoparticle (Fig. 1). This oscillation is known as the surface plasmon resonance (SPR)[22,24,25,32-34]. The resonance lies at visible

Mie theory for homogenous spherical nanoparticles

Mie theory predicts the optical properties of homogenous spherical particles. For very small particles of radius *R* (where $2R << \lambda$, and λ is the wavelength of light), the extinction cross-section can be expressed as:

$$C_{ext} = \frac{24\pi^2 R^3 \varepsilon_m^{3/2}}{\lambda} \frac{\varepsilon''}{(\varepsilon'+2\varepsilon_m)^2+\varepsilon''^2} \quad (1)$$

where $\varepsilon = \varepsilon'(\lambda) + i\varepsilon''(\lambda)$ is the wavelength-dependent, complex dielectric function of the nanoparticle material and ε_m is the dielectric constant of the surrounding/embedding medium. Eq 1 predicts an extinction maximum at wavelength λ where $\varepsilon' = -2\varepsilon_m$, the SPR condition. When this condition is fulfilled, the light field induces a resonant coherent dipolar oscillation of free electrons across the nanoparticle. For nanoparticles of Ag, Au, and Cu, the resonance condition is satisfied at visible wavelengths. This is the origin of their intense colors[22,29].

frequencies for the noble metals Au, Ag, and Cu[34]. The surface plasmon oscillation of the metal electrons results in a strong enhancement of absorption and scattering of electromagnetic radiation in resonance with the SPR frequency of the noble metal nanoparticles, giving them intense colors and interesting optical properties[31,32]. The frequency and cross-section of SPR absorption and scattering is dependent on the metal composition[35], nanoparticle size and shape[33,34,36,37], dielectric properties of the surrounding medium/substrate[25,38,39], and presence of inter-particle interactions[40-43].

Au and Ag are the plasmonic metals of choice because of their much higher stability as compared to Cu. Further, spherical Au colloids can easily be made in a wide range of sizes (4-80 nm) by facile chemistry involving the reduction of Au ions in solution[44]. Other interesting Au nanostructures (Fig. 2) with modified optical properties, e.g. nanorods[45-48], nanoprisms[49], triangular nanoparticles[50], nanocubes[51], and composite silica core-Au shell particles[52], can

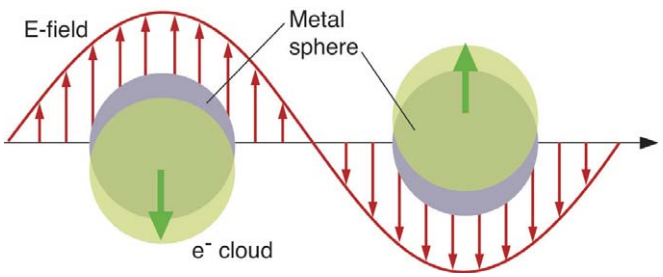

Fig. 1 Schematic of the interaction of a metal nanosphere with light. The electromagnetic field of the light induces a coherent dipolar oscillation of the metal conduction electrons across the nanoparticle. (Reprinted with permission from[25]. © 2003 American Chemical Society.)

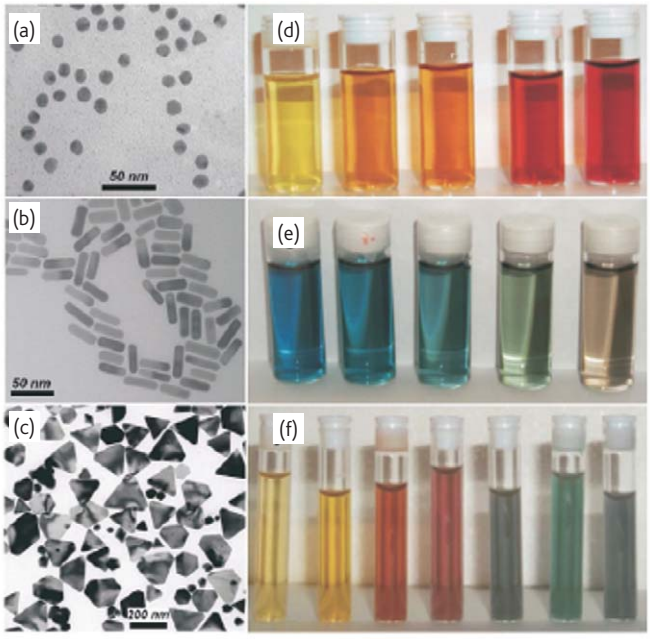

Fig. 2 Synthetic tunability of noble metal nanoparticles. (Left) Transmission electron micrographs of (a) Au nanospheres, (b) Au nanorods, and (c) Ag nanoprisms. (Right) Photographs of colloidal dispersions of (d) AuAg alloy nanoparticles with increasing Au concentration, (e) Au nanorods of increasing aspect ratio, and (f) Ag nanoprisms with increasing lateral size. (Reprinted with permission from[53]. © 2004 Elsevier.)

be fabricated via wet synthesis techniques, electrochemistry[54], photochemical techniques[55,56], or nanolithography[57,58].

Advantages of Au nanoparticles as contrast agents in biomedicine

Current diagnostic and investigational techniques in molecular biology and biomedicine rely heavily on chemical contrast agents to stain/label specific cells and tissues of interest[59] in order to overcome the problem of weak optical signals of endogenous chromophores and the subtle spectral differences between normal and diseased cells and tissues[60]. Early optical contrast agents were based on absorbing and fluorescing dyes such as malachite green and rhodamine-6G[61]. However, organic dyes suffer from rapid photobleaching[62], thus motivating the recent use of semiconductor quantum dots with intense size-dependent photoluminescence in biological and cell imaging[63,64]. The potential human toxicity and cytotoxicity of the semiconductor material, however, limits *in vitro* and *in vivo* use of quantum dots.

Colloidal Au nanoparticles with strong surface-plasmon-enhanced absorption and scattering are an important addition to the toolbox of imaging labels and contrast agents[15-18]. Immunogold nanoparticles conjugated to antibodies and Fab fragments have been used since the 1980s for biological labeling and staining in electron microscopy based on their charged properties[65,66]. Au nanoparticles are not susceptible to photobleaching and they appear biocompatible and noncytotoxic, as supported by recent experiments on human cells[67]. Further, colloidal Au has been used as a radioactive label *in vivo* since the 1950s[68]. The use of nontoxic and biocompatible nanoparticle-capping materials is nevertheless crucial for medical applications. Further, toxicity can be reduced by selectively targeting the diseased cells and tissues.

Another factor motivating the use of Au nanoparticles is their facile bioconjugation and biomodification[4]. The Au nanoparticle surface has a strong binding affinity towards thiols, disulfides, and amines[4,69]. In particular, the simple Au-thiol chemistry allows the surface conjugation[4,69] of various peptides, proteins, and DNA, either via a naturally available thiol group such as cysteine[70] or a synthetically incorporated thiol group as in case of thiolated single-stranded DNA[71]. Electrostatic adsorption of biomolecules, such as vitamin C[72] or large protein/enzyme molecules[73], to the nanoparticle surface is a simple and commonly employed technique for Au nanoparticles capped with citrate or similar carboxylic acid derivatives[4]. Functionalization of Au nanoparticles with antibodies[15,17], biomolecules such as folate (avidly taken up by cancer cells)[74], and even viruses[75] allows for the selective targeting of cancer cells. Surface modification with thiolated poly(ethylene glycol) (PEG) passivates nanoparticles and masks them from the intravascular immune system, allowing increased blood circulation times[76]. Unlike organic molecules or dyes, multiple functionalities can also be incorporated onto the same nanoparticle, making them superior for targeted drug delivery applications[8].

Tunable optical properties

Due to the phenomenon of SPR, the absorption and scattering cross-sections of Au nanoparticles are significantly superior to the absorbing and fluorescing dyes conventionally used in biological and biomedical imaging[14]. Mie theory allows for easy estimation and characterization of metal nanoparticle optical properties. For example, Mie theory[25,37] estimates that the optical cross-sections of the Au nanospheres are typically four to five orders of magnitude higher than those of conventional dyes[37]. That is, Au nanospheres with a diameter of 40 nm have a calculated molar absorption coefficient (ε) of ~7.7 x 10^9 M^{-1} cm^{-1} at a wavelength maximum around 530 nm[37], four orders of magnitude larger than the extinction coefficient for rhodamine 6G (ε =1.2 x 10^5 M^{-1} cm^{-1} at 530 nm)[77] and malachite green (ε = 1.5 x 10^5 M^{-1} cm^{-1} at 617 nm)[77]. Furthermore, Mie scattering calculations[37] show that the magnitude of visible light scattering by plasmon resonant Au nanoparticles of 80 nm diameter (C_{sca} ~ 1.2 x 10^{-14} m^2 at 560 nm) is comparable to the scattering at the same wavelength from the much larger 300 nm polystyrene nanospheres (C_{sca} ~ 1.8 x 10^{-14} m^2) commonly used in confocal imaging of cells[78]. Also, for the same light excitation intensity, the number of photons emitted by fluorescein, a fluorescent molecule commonly used in imaging (emission coefficient ~ 9.2 x 10^4 M^{-1} cm^{-1} at 483 nm, assuming unity quantum yield)[77], is five orders of magnitude lower than the light scattering from 80 nm Au nanospheres (molar scattering coefficient ~ 3.2 x 10^{10} M^{-1} cm^{-1} at 560 nm)[37].

The effectiveness of nanoparticles as contrast agents depends on their optical properties[37]. For instance, a high scattering cross-section is essential for cell and biomedical imaging applications based on light scattering. On the other hand, applications using light absorption require a high nanoparticle absorption cross-section along with low scattering losses.

Unlike conventional dyes, the optical absorption and scattering properties of Au nanoparticles can be tuned by changing their size and shape[22,25,33,36-38,79]. Fig. 3 shows the absorption, scattering, and extinction spectra of Au nanospheres of different sizes, calculated using Mie theory. Au nanospheres with a diameter of 20 nm show essentially only surface plasmon enhanced absorption with negligible scattering (Fig. 3a)[37]. However, when the particle diameter is increased from 20 nm to 80 nm, the relative contribution of surface plasmon scattering to the total extinction of the particle increases (Fig. 3). The increase in the ratio of scattering to absorption with nanoparticle volume thus provides a tool for nanoparticle selection for contrast applications. For instance, larger nanoparticles are more suitable for light-scattering-based imaging applications.

The wavelength of plasmon-enhanced absorption and scattering can also be tuned by changing the nanoparticle size and shape[25,33,36,80]. For instance, a colloidal solution of Au nanospheres with a diameter of 20 nm possesses an intense ultraviolet-visible (UV-vis) light extinction band centered on 520 nm, characteristic of their deep red color. This SPR band shifts to higher wavelengths with increasing nanoparticle diameter (Fig. 3d)[37,80]. Thus, the color of Au nanoparticles can be tuned by changing their size, though this is limited to the visible region of the electromagnetic spectrum. The effect of Au nanoparticle shape on optical properties is much more dramatic, as discussed later.

Another interesting property of Au nanoparticle SPR is its sensitivity to the local refractive index/dielectric constant of the environment surrounding the nanoparticle surface[12,25,39]. The nanosphere plasmon resonance shifts to higher wavelengths with increasing refractive index of the medium[35]. This phenomenon has been explored in the sensing of biomolecular analytes by monitoring a change in the SPR wavelength with the occurrence of an adsorption/binding event at the surface of Ag or Au nanoparticles[12,13]. The nanoparticle SPR can also be red-shifted by the self-assembly or aggregation of particles[40-43].

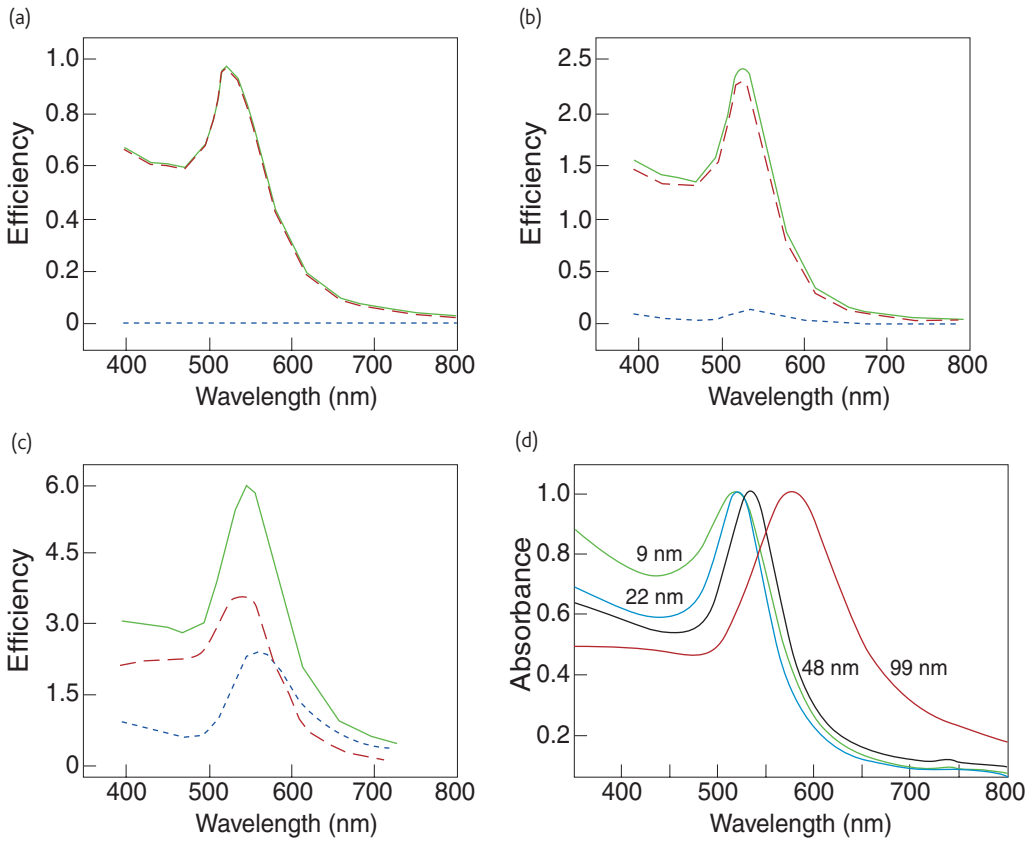

Fig. 3 Mie theory absorption (red dashed curve), scattering (blue dotted curve) and extinction (green solid curve) spectra of Au nanospheres of diameter (a) 20 nm, (b) 40 nm, and (c) 80 nm. Spectra are shown in terms of efficiency, which is the ratio of the calculated optical cross-section of a nanoparticle to its actual geometrical cross-section. (d) UV-vis extinction spectra of colloidal solutions of Au nanoparticles of different diameters varying from 9-99 nm. (Parts (a)-(c) reprinted with permission from[37]. © 2006 American Chemical Society. Part (d) reprinted with permission from[80]. © 1999 American Chemical Society.)

Cancer cell imaging using Au nanoparticle bioconjugates

Cancer diagnosis/detection using current optical imaging technologies such as optical coherence tomography (OCT) and reflectance confocal microscopy (RCM) is based on the imaging of microanatomical features of diseased tissue[15,81-83], with limited ability to image molecular changes associated with carcinogenesis[15]. A significant advantage, especially from the point of view of early detection and therapeutic progress, is achieved by the use of cancer biomarkers[84] and optical contrast agents[78], which provide a strong source of molecular specific signal from the cancerous tissue and so give both molecular and anatomical features of the disease.

The intense surface-plasmon-enhanced scattering from Au nanoparticles makes them promising as optical probes and labels for imaging-based detection of cancers[15,17]. Diseased cells can be characterized and differentiated by a range of possible alterations in their DNA, respiratory pathway, cell-surface receptor profile, or proteomic profile. One such technique for molecular specific labeling of cancer cells is the immunotargeting of nanoparticles by conjugating them with antibodies to antigens overexpressed on the diseased cells.

Sokolov *et al.*[15] employed immunotargeted Au nanoparticles for the imaging of cervical epithelial cancer cells (SiHa cells) known to overexpress the transmembrane glycoprotein, epithelial growth factor receptor (EGFR) in comparison with healthy cells[85]. Colloidal Au nanoparticles ~12 nm in diameter were conjugated to anti-EGFR monoclonal antibodies via noncovalent electrostatic adsorption of the antibody molecules to the citrate-capped, negatively-charged Au nanoparticle surface[15]. The surface adsorption of anti-EGFR antibody molecules results in a ~6 nm redshift in the UV-vis absorption band of the ~12 nm Au colloid, confirming antibody binding.

The cell suspensions were labeled with the Au nanoparticle-antibody conjugates by simple incubation. Using a scanning confocal reflectance microscope, with a 647 nm laser to excite the nanoparticle SPR, SPR scattering of the Au nanoparticles labeling the cells was clearly demonstrated on an otherwise dark background (Fig. 4)[15]. The scattering from unlabeled SiHa cells was ~50-fold lower and they could not be identified on a dark background. Similarly, no labeling was observed in the case of Au nanoparticles conjugated with bovine serum albumin (BSA) molecules, which have no specific binding to the epithelial cell surface. The SPR scattering images, in comparison with transmittance images of the same cell sample obtained independently, show that binding of the nanoparticle-antibody conjugates occurs mainly on the surface of the cell cytoplasmic membrane, confirming the molecular specificity of the labeling technique. Laser scanning reflectance microscopy of abnormal cervical cancer biopsies labeled with the anti- EGFR/nanoparticle conjugates clearly shows nanoparticle scattering from the cytoplasmic membrane region of the cells, while normal biopsies show no labeling under similar acquisition conditions (Fig. 5)[15].

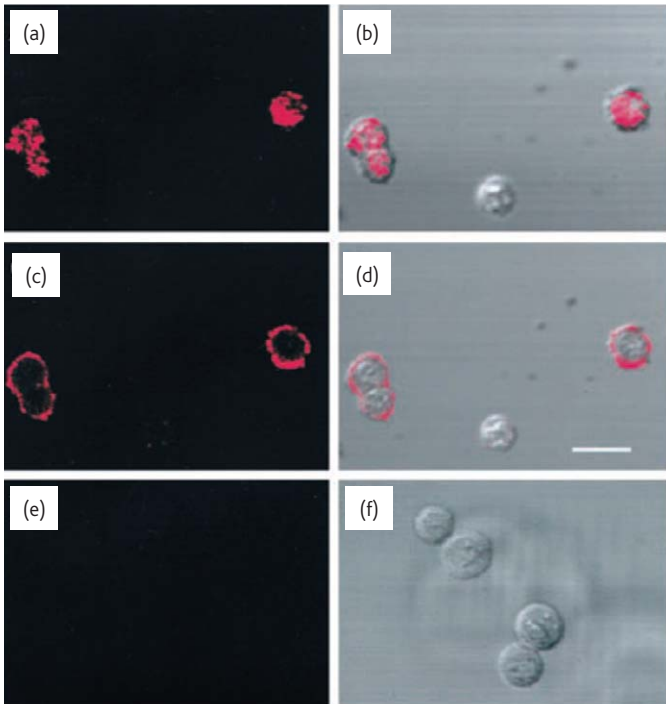

Fig. 4 (a)-(d) Optical images of SiHa cells labeled with anti-EGFR/Au conjugates. (e),(f) Nonspecific labeling using anti-EGFR/Au conjugates with BSA. Laser scanning confocal reflectance (a), (c), and (e) and combined confocal reflectance/transmittance (b), (d), and (f) images of the labeled SiHa cells obtained with 40x objective. The scattering from the nanoparticle bioconjugates is false-colored in red. In (a) and (b), the focal plane is at the top of the cells. In (c) and (d), the middle cross-section of the cells is in focus. The combined confocal reflectance/transmittance images were obtained independently and then overlaid. Reflectance images were obtained with 647 nm laser excitation. Scale bar = ~20 μm. (Reprinted with permission from[15]. © 2003 American Association for Cancer Research.)

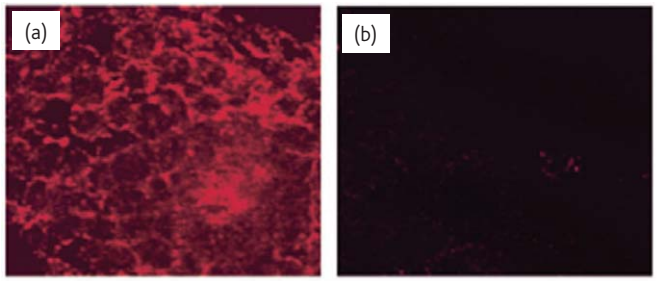

Fig. 5 Laser scanning confocal reflectance images of (a) precancerous and (b) normal fresh cervical ex vivo tissue labeled with anti-EGFR/Au nanoparticle bioconjugates. The images were obtained with 647 nm excitation wavelength, and are false-colored in red. (Reprinted with permission from[15]. © 2003 American Association for Cancer Research.)

The researchers also demonstrated that SPR scattering from the Au nanoparticles is strong enough to allow use of a red laser pointer *in lieu* of the scanning laser to image the labeled cancer cells[15]. Thus the use of Au bioconjugates has potential for cancer diagnosis even in resource-poor settings.

While SPR scattering is intense, as demonstrated by Sokolov *et al.*[15], it is also self-selecting and can therefore be used with a broad

spectrum excitation source. An extremely simple and inexpensive technique using dark-field microscopy under white light illumination has been recently demonstrated by El-Sayed *et al.*[17] for the successful detection and differentiation of cancerous cells from noncancerous cells. The technique uses SPR scattering imaging and SPR absorption spectroscopy of ~35 nm Au nanoparticles conjugated with anti-EGFR antibodies immunotargeted to two malignant epithelial cell lines (human oral squamous carcinomas, HOC 313 clone 8 and HSC 3). A nanoparticle size of 35 nm was chosen to obtain the optimum light scattering enhancement. Under white light excitation, only the light frequency corresponding to the SPR maximum is scattered intensely, resulting in an image of colored nanoparticles on a dark background. Light scattering images of the cancerous HOC and HSC cells labeled with the anti-EGFR/Au nanoparticle conjugates were obtained on a conventional microscope under dark-field white light illumination. The labeled cancer cells are clearly defined on a dark background (Fig. 6) by the intense SPR scattering from the nanoparticle conjugates, which accumulate in the cytoplasmic membrane regions because of the specific binding of the antibodies to EGFR overexpressed on the surface of the malignant cells[17]. In comparison, benign keratinocyte cell lines (HaCaT) incubated with the Au bioconjugates show no specific labeling. Instead, a random distribution of nanoparticles over the HaCaT cells and extracellular matrix is seen because of nonspecific interactions, without defining the cell surface.

In addition, the strong SPR absorption of Au nanoparticle bioconjugates provides a novel method for sensing and quantifying the molecular specific nanoparticle labeling by microabsorption spectroscopy. The microabsorption spectra of the labeled HOC and HSC cells shows an SPR absorption band maximum around 545 nm, which is red-shifted by 9 nm from that of the isolated anti-EGFR/Au nanoparticles in solution (Fig. 6)[17]. The red shift is a result of the change in the local dielectric environment around the nanoparticle as the conjugated antibody binds to its target, thus providing an additional ability for sensing molecular activity. The specific and homogeneous binding of antibody-conjugated nanoparticles to the cancer cell surface results in a sharper SPR absorption band for the

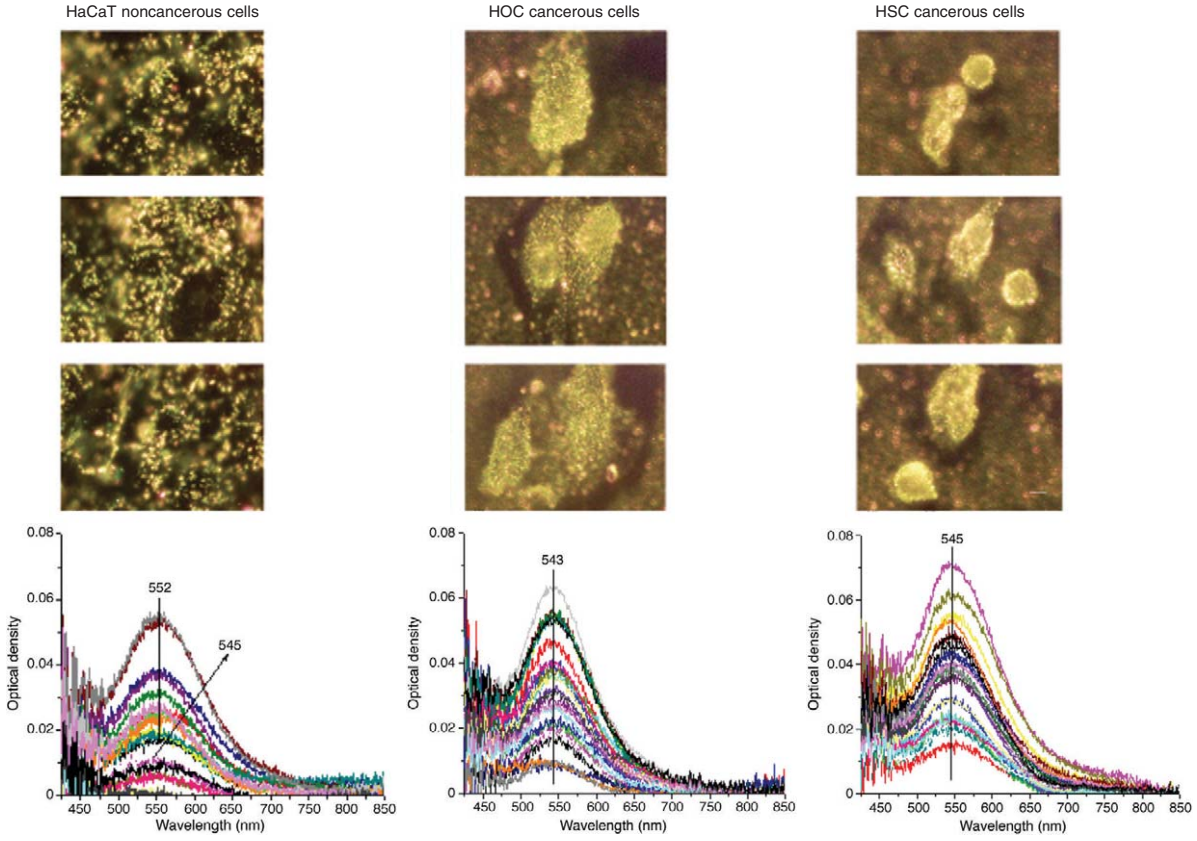

Fig. 6 Two simple techniques for sensitive cancer diagnosis using anti-EGFR/Au nanoparticle bioconjugates: white light, dark-field microscopy (top three rows) and microabsorption spectrometry (bottom row). Light scattering images and microabsorption spectra are shown for HaCaT noncancerous cells (left column), HOC cancerous cells (middle column), and HSC cancerous cells (right column) after incubation with the nanoparticle bioconjugates. Three different images of each kind of cell are presented to show reproducibility. The microabsorption spectra were measured for 25 different cells. Clear differences can be seen in the scattering images and absorption spectra for noncancerous (left column) and cancerous cells (right two columns). This is the result of specific binding of the nanoparticle bioconjugates in high concentrations to the surface of the cancer cells, while the noncancerous cells remain relatively unlabeled. Scale bar = 10 μm. (Reprinted with permission from[17]. © 2005 American Chemical Society.)

cancerous cells compared with that of noncancerous cells, where the nanoparticles are bound nonhomogenously through nonspecific interactions. The absorption intensity provides a direct measure of the number of bound nanoparticles and can be used to quantify the labeled biomarker profiles. Based on the absorption intensity of the labeled cells at the SPR wavelength maximum, we conclude that the Au nanoparticle bioconjugates specifically bind to the surface of the cancerous cells with six times greater affinity than to noncancerous cells[17]. The absorption intensity even shows subtle differences for the two cancer cell types (HOC and HSC), indicating dissimilarity in the number of bound antibody/antigen complexes. These results correlate well with the relative number of receptors present on the cell surface of the three cell lines, as estimated by biological techniques. Thus we have successfully exploited the SPR scattering and absorption of anti-EGFR/Au bioconjugates to differentiate cancerous cells from healthy cells based on overexpression of surface EGFR[17]. The technique can be extended to other forms of cancer or precancer by employing an immunotargeting scheme specific to particular biomolecular signatures. Furthermore, simultaneous multicolor imaging of multiple targets can be achieved with a single white light source by plasmonic nanoparticles of different sizes and shapes conjugated to different probe molecules. This removes the need for complex photoprocessing and image overlaying common in multicolor fluorescent probe techniques. The use of Au nanoparticle contrast agents with well-established and

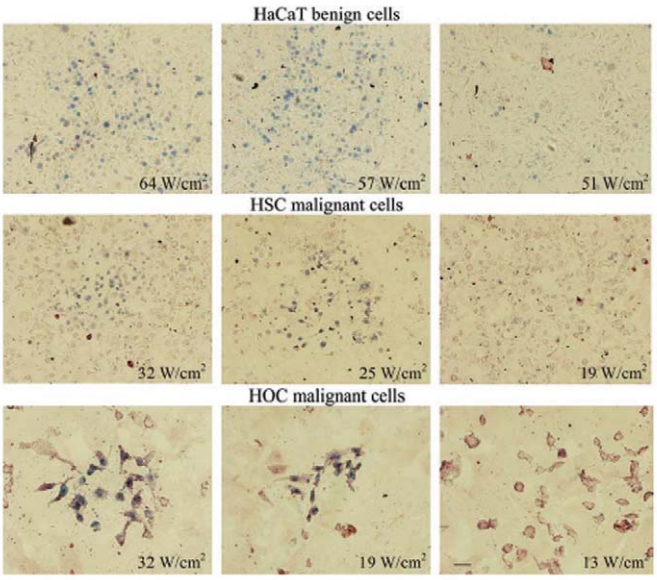

Fig. 7 Selective photothermal damage of cancer cells using anti-EGFR/Au nanoparticle bioconjugates and exposure for 4 min to weak CW laser radiation at the nanoparticle SPR absorption frequency. Bright-field microscopy images (10x objective) of benign HaCaT cells (top row), malignant HSC cells (middle row), and malignant HOC cells (bottom row) irradiated at different laser powers and then stained with trypan blue. Benign HaCaT cells are killed at and above 57 W/cm², malignant HSC cells are killed at and above 25 W/cm², and malignant HOC cells are killed at and above 19 W/cm². Scale bar = 60 μm. (Reprinted with permission from[98]. © 2006 Elsevier Ltd.)

developing optical imaging techniques (e.g. OCT, RCM[15], photoacoustic tomography[86], multiphoton plasmon resonance microscopy[16], optical coherence microscopy[87], and third-harmonic microscopy[88]) holds further promise for imaging cancer at the cellular or molecular level.

Selective photothermal cancer therapy using Au nanoparticle bioconjugates

Mainstream treatments for most forms of cancer (epithelial cancers) include surgical tumor removal, chemotherapy, and radiation therapy. However, surgery is limited to tumors that are accessible[89], chemotherapy suffers from problems arising from side effects[90], and radiotherapy is highly invasive to healthy tissue in the path of the radiation[91]. In the face of these drawbacks, laser hyperthermia, i.e. use of optical heating for ablation of tumors, offers a gentler alternative for cancer treatment[92,93]. By employing strong photoabsorbers such as dyes[94,95] that are located selectively in the tumor region, the speed and effectiveness of the heat deposition can be greatly enhanced while reducing nonspecific injury to adjacent healthy tissue.

The SPR absorption of Au nanoparticles is followed by the rapid conversion (~1 ps) of the absorbed light into heat[23,33,34,36,96]. The ability of Au nanoparticles to convert strongly absorbed light efficiently into localized heat can be exploited for the selective photothermal therapy of cancer[97-102] and bacterial infection[103]. Selective targeting of nanoparticles to biomarkers on cancer cells[98-100,102] increases the specificity of labeling and decreases the laser dose needed to kill diseased cells, without injuring healthy cells. The absorption cross-section of Au nanoparticles (C_{abs} ~ 2.9 x 10^{-15} m^2 for 40 nm spheres with an absorption band around 530 nm)[37] is five orders of magnitude larger than that of indocyanine green (C_{abs} ~ 1.7 x 10^{-20} m^2 around 800 nm)[104], a dye used in earlier demonstrations[94,95] of laser photothermal tumor therapy, thus promising effective photothermal therapy at much lower irradiation energy. Besides, selection of a plasmonic nanoparticle configuration with optimum SPR absorption as well as SPR scattering makes a dual imaging/therapy approach possible.

El-Sayed *et al.*[98] recently showed the efficiency of immunotargeted Au nanospheres as photothermal agents in living cells *in vitro*. As discussed previously[17], two oral squamous carcinoma cell lines, HOC and HSC, that overexpress EGFR protein can be labeled effectively using 40 nm Au nanoparticles conjugated to anti-EGFR antibodies. Dark-field microscopy images of the SPR scattering from the nanoparticles provide visual confirmation of the labeling of the cancer cell surface, while healthy HaCaT cells show relatively nonspecific nanoparticle labeling[98]. For photothermal therapy, 514 nm excitation from a commonly available continuous-wave (CW) argon-ion laser was used to excite the SPR band of the nanoparticles centered on 530 nm and ensure maximum light absorption by the nanoparticles. To test the viability of cells following photothermal irradiation, they were stained with trypan blue dye, which accumulates selectively in dead cells staining them blue, while live cells remain clear in

microscope images (Fig. 7)[98]. The cancerous HOC and HSC cells suffer photothermal damage within 4 mins at laser energy thresholds (19 W/cm^2 and 25 W/cm^2), which are less than half that of healthy HaCaT cells (57 W/cm^2). None of the cell lines without Au nanoparticle treatment showed any photothermal damage up to laser energies of 76 W/cm^2. Thus effective targeting of Au nanoparticle bioconjugates specifically to cancer cells, combined with the high absorption cross-section of the nanoparticles in the laser excitation region, facilitates selective photothermal cancer therapy at a low enough laser energy that the benign cells remain undamaged[98,102].

Near-infrared imaging and therapy

The *in vitro* success of cancer therapy/imaging using visible light absorbing nanoparticles can be extended to skin or surface type cancers. However, *in vivo* imaging and photothermal therapy applications for deeper tissue require light in the near-infrared (NIR) region where tissue (hemoglobin and water) has the highest transmissivity[105]. The light penetration depth can be up to a few centimeters in the spectral region 650-900 nm, also known as the biological NIR window, depending on the tissue type[105]. Thus the plasmon resonance of nanoparticles for *in vivo* applications is required to be in the NIR region. While changing the size of Au nanospheres shows limited tunability of the SPR wavelength[33,37,80], changing the Au nanoparticle shape[23,25,33,34,36,37] and composition[52,60] offers dramatic variation in SPR absorption and scattering properties. Interesting nanostructures, such as silica-Au nanoshells[52,60], Au nanorods[79,106-108], Au nanocages[109], and Au nanoparticle assemblies[100] show optical tunability in the NIR region suitable for *in vivo* applications. An alternative method is to achieve the controlled self-assembly of Au nanoparticles on a cell membrane, which results in a red shift of the SPR frequency to the NIR[100,110].

Tuning SPR in the NIR: silica-Au nanoshells

Halas and coworkers[52,60] have achieved the desirable optical tunability using composite particles with a silica core and a thin Au shell, which are also known as nanoshells. Silica nanoparticles can be grown in a range of sizes by the Stober method[111] , then the Au shell can be grown following the method of Duff *et al.*[112]. By varying the relative core and shell thickness of the Au nanoshells, their SPR can be varied across a broad wavelength range that extends from the visible to the NIR region (Fig. 8)[52,60,113]. Nanoshells can thus be synthetically designed to have high SPR scattering and/or absorption in the NIR region facilitating *in vivo* optical imaging and therapy.

Hirsch *et al.*[97] have shown that human breast carcinoma cells incubated with nanoshells (55 nm silica core, 10 nm thick Au shell) possessing SPR extinction centered on 800 nm undergo photothermal damage on exposure to NIR laser light (820 nm, 4 W/cm^2, 7 min). The *in vitro* success of NIR therapy has been extended *in vivo* by direct injection of thiolated PEG-coated silica-Au nanoshells into mice

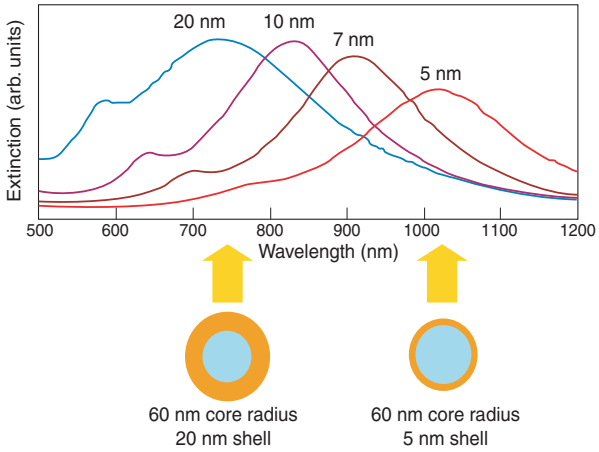

Fig. 8 SPR extinction of silica core-Au shell nanoshells as a function of their core/shell thickness ratio. The SPR wavelength red-shifts with increasing core/shell ratio, allowing tunability of the nanoshell absorption and scattering in the NIR region. (Reprinted with permission from[60]. © 2004 Adenine Press.)

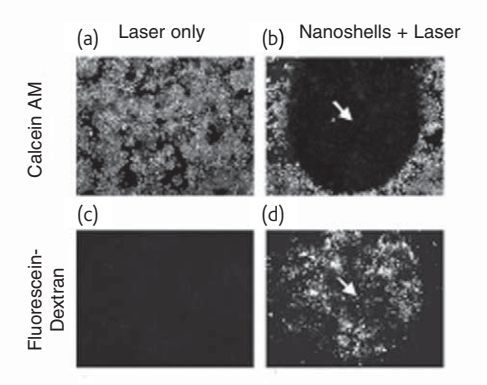

Fig. 9 Cells irradiated in the absence of nanoshells maintain both viability, as depicted by (a) calcein fluorescence, and membrane integrity, as indicated by (c) lack of intracellular fluorescein dextran uptake. Cells irradiated with nanoshells possess well-defined circular zones of cell death, as shown by (b) the calcein fluorescence study and (d) cellular uptake of fluorescein dextran resulting from increased membrane permeability. (Reprinted with permission from[97]. © 2003 National Academy of Sciences.)

tumors[97]. The surface PEG layer provides stability against nanoparticle agglomeration in physiological solutions. Low doses of NIR laser light (820 nm, 4 W/cm^2, 4-6 min) result in high temperatures localized in the tumor regions (ΔT = 37.4 + 6.6°C as shown by magnetic resonance temperature imaging), enough to induce irreversible tissue damage (Fig. 9)[97]. Laser doses for successful therapy were 10- to 25-fold less than used in earlier studies[94,95] with an NIR-absorbing dye. Control tissues exposed to NIR light without nanoshell injections show a much lower temperature rise (ΔT < 10°C) without any tissue damage.

In further experiments[99] on breast carcinoma cells *in vitro*, NIR laser photothermal therapy was rendered more selective by molecular specific labeling of the cancer cells with nanoshells conjugated with antibodies to HER2, a protein overexpressed in breast cancer cells.

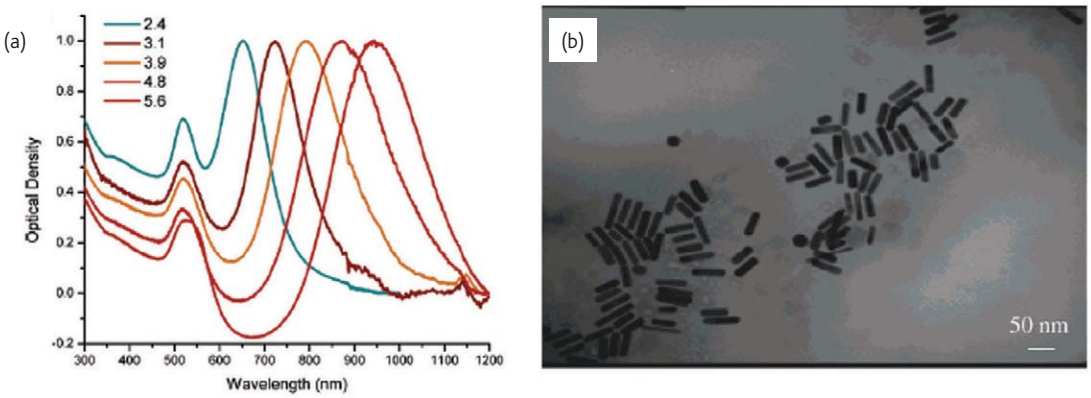

Fig. 10 (a) SPR extinction spectra of Au nanorods with different aspect ratios showing the sensitivity of the strong longitudinal SPR band to the aspect ratio. The longitudinal SPR band red-shifts with increasing aspect ratio, which allows optical tunability in the NIR region. (b) Transmission electron micrograph of a sample of Au nanorods with an average aspect ratio of ~3.9, the extinction spectrum of which is shown as the orange curve in (a). (Reprinted with permission from[107]. © 2006 American Chemical Society.)

Tuning SPR in the NIR: Au nanorods

Another strategy to achieve NIR imaging and therapy is to use rod-shaped nanoparticles composed of Au, thus removing the use of potentially carcinogenic silica material in nanoshells. It is well known that by changing the shape of Au nanoparticles from spheres to elongated rods, the optical characteristics can be significantly changed[23,33,34,36,108,114]. Au nanorods possess, in addition to an SPR band around 530 nm that corresponds to the transverse plasmon oscillation, a stronger band at longer wavelengths arising from the plasmon oscillation of electrons along the longitudinal axis of the nanorods[23,33,34,36,108,114]. It has been well established that the longitudinal plasmon resonance maximum can be shifted into the NIR region by an increase in the nanorod aspect ratio, i.e. the ratio of length along the long axis to the short axis (Fig. 10)[33,34,36,37,107,108]. Au nanorods with controlled aspect ratios in the range of 2-6 (corresponding to SPR bands in the 600-1000 nm region) can be synthesized via the micelle-templated seed and feed method developed by the Murphy group[45,46,48,115] and improved by Nikoobakht and El-Sayed[47]. Fig. 11 shows calculated spectra of the extinction, absorption, and scattering efficiency of Au nanorods of different aspect ratios based on electrodynamic simulations by Lee *et al.*[79].

Recently, Huang *et al.*[107] employed Au nanorods conjugated to anti-EGFR antibodies for NIR cancer cell imaging and selective photothermal therapy. Au nanorods with an average aspect ratio of

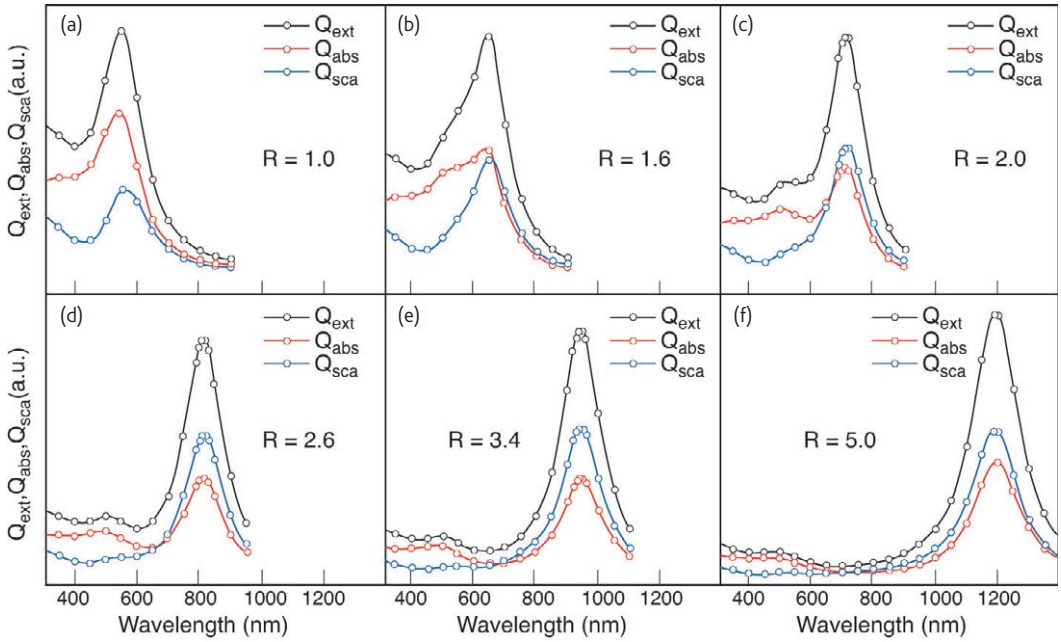

Fig. 11 Electrodynamic simulations of spectra for SPR extinction, absorption, and scattering efficiencies of Au nanorods with increasing aspect ratio from (a) to (f). (Reprinted with permission from[79]. © 2005 American Chemical Society.)

~3.9 showing a strong longitudinal absorption band around 800 nm were used (Fig. 10)[107]. As a result of intense red scattering from the Au nanorods, malignant HOC and HSC cells labeled with the nanorod bioconjugates were clearly seen in optical microscopy images under dark-field white light illumination, allowing their differentiation from nonmalignant HaCaT cells (Fig. 12a)[107]. Note that red scattering from the Au nanorods is in stark contrast to the green-yellow scattering from spheres (Fig. 6)[17].

Following light-microscopy-based detection of the cancer cells, the labeled cells were exposed for 4 mins to a continuous wave Ti:sapphire laser at 800 nm having a strong spectral overlap with the intense longitudinal SPR absorption band of the nanorods. The results (Fig. 12b) show that the laser energy threshold for photothermal damage of the labeled malignant cells (10 W/cm^2) is nearly half that for nonmalignant cells (20 W/cm^2) incubated with the same nanoparticles[107].

It is known that many solid tumors, including brain, bladder, stomach, breast, lung, endometrium, cervix, vulva, ovary, esophagus, stomach, prostate, renal, pancreatic, glioblastoma, and squamous cell carcinoma cells, overexpress EGFR on the cell cytoplasmic membrane to different degrees[116]. This can be exploited for the selective delivery of anti-EGFR/Au nanorod bioconjugates in high concentrations to cancer cells, followed by simultaneous NIR cancer diagnosis and selective photothermal therapy[107]. Besides SPR scattering and absorption, the Au nanorods also show strongly enhanced fluorescence allowing *in vivo* imaging using a two-photon NIR excitation scheme[117].

Delivering Au nanoparticles to the tumor site

For *in vivo* imaging/therapy applications, the selective delivery of Au nanoparticles to the tumor site is crucial, and several strategies have been proposed. Possible routes of delivery include topical application to epithelial tumors and injection into tumor beds using a needle (for

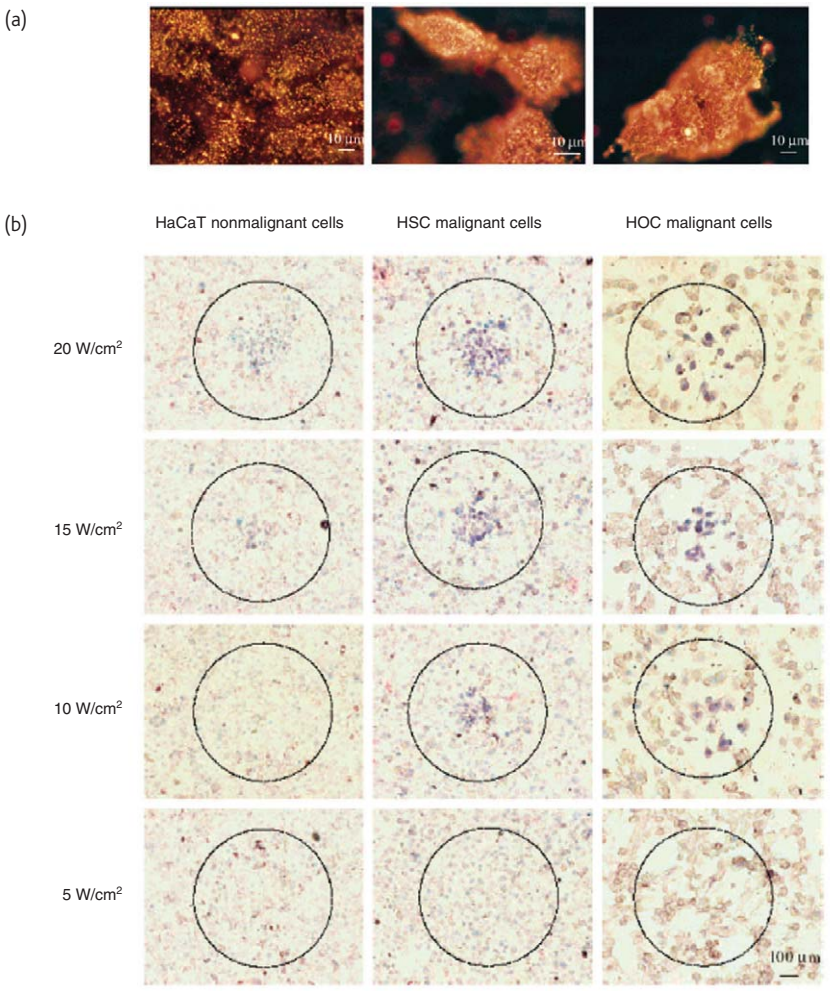

Fig. 12 (a) Light scattering images of HaCaT (left), HSC (middle), and HOC (right) cells labeled with anti-EGFR/Au nanorod bioconjugates. (b) Selective photothermal therapy of cancer cells labeled with anti-EGFR/Au nanorod bioconjugates. The circles show the laser spots on the samples. At 10 W/cm^2, the HSC (middle) and HOC (right) malignant cells show clear injury while the HaCaT normal cells are not affected. The HaCaT normal cells begin to be injured at 15 W/cm^2 and are obviously injured at 20 W/cm^2. (Reprinted with permission from[107]. © 2006 American Chemical Society.)

physically accessible tumors), intravascular injection and intraoperative application into residual tumor or suspect areas. In regions with vital structures nearby, as in skull base surgery, residual tumor is often left and represents a prime target for intraoperative application.

Intravascular injection is attractive because it offers the possibility of catching every tumor cell in the body. Many solid tumors possess highly permeable, poorly organized vascular networks[118]. Nanoparticles and macromolecules in the size range of 60-400 nm accumulate preferentially within many of these solid tumors as a result of extravasation from the blood circulation[119]. This effect is also known as the enhanced permeability and retention effect[120]. A current technology under human trial by Cytimmune Sciences employs PEG-coated Au nanoparticles as carriers of anticancer chemotherapeutics[8,121]. The PEG coating renders the nanoparticles biocompatible, minimizes their agglomeration, and masks them from the immune system[122]. As a result, PEG-passivated nanoparticles injected intravenously exhibit a higher retention time in the blood and preferentially accumulate within many solid tumor beds[97,123]. Similarly, O'Neal *et al.*[123] have shown that the injection of PEG-coated nanoshells into mice via their tail vein results in preferential accumulation in the tumor region within six hours. Subsequent NIR irradiation of the tissue results in selective ablation of the nanoparticle-enriched tumor regions leaving the surrounding healthy tissue intact[123].

Other intravascular targeting strategies exist. Functionalization of nanoparticles with ligands directed to overexpressed antigens is an exciting possibility. Recently, monoclonal antibody therapy has proven its efficacy for a host of tumors[124,125], demonstrating that the antibodies can localize within tumors and result in increased uptake of immunotargeted nanoparticles. Conjugation of nanoparticles to viral vectors is also being pursued, based on the successful targeting of viral vectors to tumors with potential for dual gene/photothermal therapy[75].

Conclusion and future outlook

The strongly enhanced SPR scattering and absorption of Au nanoparticles makes them a novel and highly effective class of contrast agents for biological and cell imaging-based cancer diagnostics and photothermal cancer therapy[15,17,97-99,107]. Molecular specific imaging and therapy of cancer is achieved by the synthetic conjugation of the nanoparticles with antibodies targeted to receptors overexpressed on the cancer cells[15,17,98,99,107]. By employing appropriate targeting strategies, the imaging/therapy scheme can be made generic to a variety of cancers and even extended to other diseases.

Notwithstanding the success of initial demonstrations of the use of immunotargeted Au nanoparticles in cancer imaging/therapy, a number of factors need to be optimized. These include the absorption and scattering cross-sections of the nanoparticles and the binding of nanoparticles to the targeting antibodies, as well as the binding of the nanoparticle bioconjugates to cellular targets. While most studies have been conducted on cell monolayers, success in physiological environments requires attention to the pharmacokinetics of the nanoparticles, including aspects such as blood flow, permeation, tumor extravasation, physiological reactions, nanoparticle stability, etc.[119,126-128]. There is a need to study the dependence of these aspects on nanoparticle size, surface chemistry, and mode of delivery. The most effective method for delivering NIR light to the diseased cells of different cancers also needs further research. The mechanisms of nanoparticle-assisted photothermal injury of cells are also not very well understood and require further elucidation. Systematic study of all these aspects is a prerequisite for the successful translation of the research promise of plasmonic nanoparticles in cancer detection and selective photothermal therapy to a clinical setting. nt

Acknowledgments

We acknowledge the contributions of Xiaohua Huang and Wei Qian in the Laser Dynamics Lab, Georgia Institute of Technology to work included in this review, and the following people for use of their facilities and support: Paul Edmonds, Mohan Srinivasarao, Rob Dickson, Lynn Peyser, Sandeep Patel, and Jie Zheng at Georgia Institute of Technology, Randall Kramer and Oren Humstoe at the Oral Cancer Research Center, University of California, San Francisco, and Patrica Leake and Russell Snyder in the Epstein Laboratory, University of California, San Francisco. We also acknowledge the financial support of the Chemical Science, Geosciences, and Bioscience Division of the Department of Energy (NO DE-FG02-97 ER14799) for the research included here. We acknowledge the financial support of the Hearing Research Institute.

REFERENCES

1. Burda, C., *et al.*, *Chem. Rev.* (2005) **105**, 1025
2. Wang, Z. L., (ed.), *Characterization of Nanophase Materials*, Wiley-VCH, Weinheim, Germany, (2000)
3. Alivisatos, P., *Nat. Biotechnol.* (2004) **22**, 47
4. Katz, E., and Willner, I., *Angew. Chem. Int. Ed.* (2004) **43**, 6042
5. Rosi, N. L., and Mirkin, C. A., *Chem. Rev.* (2005) **105**, 1547
6. Salata, O. V., *J. Nanobiotechnol.* (2003) **2**, 3
7. Whitesides, G. M., *Nat. Biotechnol.* (2003) **21**, 1161
8. Paciotti, G., *Drug Delivery* (2004) **11**, 169
9. Suh, J., *et al.*, *Proc. Natl. Acad. Sci. USA* (2003) **100**, 3878
10. Berry, C. C., *et al.*, *Biomaterials* (2005) **26**, 4985
11. Bailey, R. C., *et al.*, *J. Am. Chem. Soc.* (2003) **125**, 13541
12. Haes, A. J., *et al.*, *J. Fluorescence* (2004) **14**, 355
13. Haes, A. J., *et al.*, *Nano Lett.* (2004) **4**, 1029
14. Yguerabide, J., and Yguerabide, E. E., *Anal. Biochem.* (1998) **262**, 157
15. Sokolov, K., *et al.*, *Cancer Res.* (2003) **63**, 1999
16. Yelin, D., *et al.*, *Opt. Exp.* (2003) **11**, 1385
17. El-Sayed, I. H., *et al.*, *Nano Lett.* (2005) **5**, 829
18. Wang, Y., *et al.*, *Nano Lett.* (2004) **4**, 1689
19. Jemal, A., *et al.*, *CA Cancer J. Clin.* (2005) **55**, 10
20. *US Mortality Public Use Data Table 2003*, National Center for Health Statistics, Center for Disease Control and Prevention, (2006)
21. Brigger, I., *et al.*, *Adv. Drug Delivery Rev.* (2002) **54**, 631
22. Kreibig, U., and Vollmer, M., *Optical Properties of Metal Clusters*, Springer, Berlin, (1995), **25**

23. El-Sayed, M. A., *Acc. Chem. Res.* (2001) **34**, 257
24. Bohren, C. F., and Huffman, D. R., *Absorption and Scattering of Light by Small Particles*, Wiley, New York, (1983)
25. Kelly, K. L., *et al.*, *J. Phys. Chem. B* (2003) **107**, 668
26. Daniel, M.-C., and Astruc, D., *Chem. Rev.* (2004) **104**, 293
27. Kerker, M., *J. Colloids Interface Sci.* (1985) **105**, 297
28. www.thebritishmuseum.ac.uk/science/text/lycurgus/sr-lycurgus-p1-t.html
29. Hutter, E., and Fendler, J. H., *Adv. Mater.* (2004) **16**, 1685
30. Faraday, M., *Philos. Trans. R. Soc. London, Ser. A* (1857) **147**, 145
31. Mie, G., *Ann. Phys.* (1908) **25**, 377
32. Mulvaney, P., *Langmuir* (1996) **12**, 788
33. Link, S., and El-Sayed, M. A., *J. Phys. Chem. B* (1999) **103**, 8410
34. Link, S., and El-Sayed, M. A., *Annu. Rev. Phys. Chem.* (2003) **54**, 331
35. Lee, K.-S., and El-Sayed, M. A., *J. Phys. Chem. B* (2006) **110**, 19220
36. Link, S., and El-Sayed, M. A., *Int. Rev. Phys. Chem.* (2000) **19**, 409
37. Jain, P. K., *et al.*, *J. Phys. Chem. B* (2006) **110**, 7238
38. Underwood, S., and Mulvaney, P., *Langmuir* (1994) **10**, 3427
39. Jensen, T. R., *et al.*, *J. Phys. Chem. B* (1999) **103**, 9846
40. Su, K.-H., *et al.*, *Nano Lett.* (2003) **3**, 1087
41. Jain, P. K., *et al.*, *J. Phys. Chem. B* (2006) **110**, 136
42. Sonnichsen, C., *et al.*, *Nat. Biotechnol.* (2005) **23**, 741
43. Jain, P. K., *et al.*, *J. Phys. Chem. B* (2006) **110**, 18243
44. Turkevich, J., *et al.*, *Discuss. Faraday Soc.* (1951) **11**, 55
45. Murphy, C. J., *et al.*, *J. Phys. Chem. B* (2005) **109**, 13857
46. Murphy, C. J., *et al.*, *Chemistry of Nanomaterials: Synthesis, Properties and Applications*, Wiley-VCH, Weinheim, Germany (2004), **1**
47. Nikoobakht, B., and El-Sayed, M. A., *Chem. Mater.* (2003) **15**, 1957
48. Murphy, C. J., and Jana, N. R., *Adv. Mater.* (2002) **14**, 80
49. Malikova, N., *et al.*, *Langmuir* (2002) **18**, 3694
50. Chen, S., and Carroll, D. L., *Nano Lett.* (2002) **2**, 1003
51. Sun, Y., and Xia, Y., *Science* (2002) **298**, 2176
52. Oldenburg, S. J., *et al.*, *Chem. Phys. Lett.* (1998) **288**, 243
53. Liz-Marzan, L. M., *Materials Today* (2004) **7** (2), 26
54. Yu, Y.-Y., *et al.*, *J. Phys. Chem. B* (1997) **101**, 6661
55. Zhou, Y., *et al.*, *Chem. Mater.* (1999) **11**, 2310
56. Eustis, S., *et al.*, *J. Phys. Chem. B* (2005) **109**, 4811
57. Hulteen, J. C., and Van Duyne, R. P., *J. Vac. Sci. Technol. A* (1995) **13**, 1553
58. Huang, W., *et al.*, *J. Phys. Chem. B* (2005) **109**, 18881
59. Grainger, R. G., *Br. J. Radiol.* (1982) **55**, 1
60. Loo, C., *et al.*, *Technol. Cancer Res. Treatment* (2004) **3**, 33
61. Bugaj, J. E., *et al.*, *J. Biomed. Opt.* (2001) **6**, 122
62. Landsman, M. L., *et al.*, *J. Appl. Physiol.* (1976) **40**, 575
63. Bruchez, Jr., M. J., *et al.*, *Science* (1998) **281**, 2013
64. Chan, W. C. W., and Nie, S., *Science* (1998) **281**, 2016
65. Hayat, M. A., *Colloidal Gold: Principles, Methods, and Applications*, Academic Press, San Diego, (1989), **1**
66. Faulk, W., and Taylor, G., *Immunochemistry* (1971) **8**, 1081
67. Connor, E. E., *et al.*, *Small* (2005) **1**, 325
68. Hultborn, K. A., *et al.*, *Acta. Radiol.* (1955) **43**, 52
69. Niemeyer, C. M., *Angew. Chem. Int. Ed.* (2001) **40**, 4128
70. Naka, K., *et al.*, *Langmuir* (2003) **19**, 5546
71. Mirkin, C. A., *et al.*, *Nature* (1996) **382**, 607
72. Rajh, T., *et al.*, *J. Phys. Chem. B* (1999) **103**, 3515
73. Broderick, J. B., *et al.*, *Biochemistry* (1993) **32**, 13771
74. Dixit, V., *et al.*, *Bioconjug. Chem.* (2006) **17**, 603
75. Everts, M., *et al.*, *Nano Lett.* (2006) **6**, 587
76. Hirsch, L. R., *et al.*, *Anal. Chem.* (2003) **75**, 2377
77. Du, H., *et al.*, *Photochem. Photobiol.* (1998) **68**, 141
78. Smithpeter, C., *et al.*, *J. Biomed. Opt.* (1998) **3**, 429
79. Lee, K.-S., and El-Sayed, M. A., *J. Phys. Chem. B* (2005) **109**, 20331
80. Link, S., and El-Sayed, M. A., *J. Phys. Chem. B* (1999) **103**, 4212
81. Collier, T., *et al.*, *Acad. Radiol.* (2002) **9**, 504
82. Tearney, G. J., *et al.*, *Science* (1997) **276**, 2037
83. Liang, C., *et al.*, *Opt. Exp.* (2001) **9**, 821
84. Grizzle, W. E., *et al.*, *Archiv. Pathol. Lab. Med.* (2001) **125**, 91
85. Maruo, T., *et al.*, *Cancer* (1992) **69**, 1182
86. Copland, J. A., *et al.*, *Mol. Imaging Biol.* (2004) **6**, 341
87. Raub, C. B., *et al.*, *Proc. IEEE Eng. Med. Biol. Soc. Conf.* (2004) **1**, 1210
88. Yelin, D., *et al.*, *Appl. Phys. B* (2002) **74** (Suppl.), S97
89. Miller, A. B., *et al.*, *Cancer* (1981) **47**, 207
90. Hamilton, A., and Hortobagyil, G., *J. Clin. Oncol.* (2005) **23**, 1760
91. Partridge, A. H., *et al.*, *J. Natl. Cancer Inst. Monogr.* (2001) **30**, 135
92. Nolsoe, C. P., *et al.*, *Radiol.* (1993) **187**, 333
93. Amin, Z., *et al.*, *Radiol.* (1993) **187**, 339
94. Chen, W. R., *et al.*, *Cancer Lett.* (1997) **115**, 25
95. Chen, W. R., *et al.*, *Cancer Lett.* (1996) **98**, 169
96. Lakowicz, J. R., *et al.*, *Proc. SPIE* (2006) **6099**, 609909
97. Hirsch, L. R., *et al.*, *Proc. Natl. Acad. Sci. USA* (2003) **100**, 13549
98. El-Sayed, I. H., *et al.*, *Cancer Lett.* (2006) **239**, 129
99. Loo, C., *et al.*, *Nano Lett.* (2005) **5**, 709
100. Zharov, V. P., *et al.*, *Lasers Surg. Med.* (2005) **37**, 219
101. Pitsillides, C. M., *et al.*, *Biophys. J.* (2003) **84**, 4023
102. Huang, X., *et al.*, *Photochem. Photobiol.* (2006) **82**, 412
103. Zharov, V. P., *et al.*, *Biophys. J.* (2006) **90**, 619
104. Urbanska, K., *et al.*, *Acta. Biochim. Pol.* (2002) **49**, 387
105. Weissleder, R., *Nat. Biotechnol.* (2001) **19**, 316
106. Brioude, A., *et al.*, *J. Phys. Chem. B* (2005) **109**, 13138
107. Huang, X., *et al.*, *J. Am. Chem. Soc.* (2006) **128**, 2115
108. Link, S., *et al.*, *J. Phys. Chem. B* (1999) 103, 3073; and correction: *J. Phys. Chem. B* (2005) **109**, 10531
109. Chen, J., *et al.*, *Adv. Mater.* (2005) **17**, 2255
110. Zharov, V. P., *et al.*, *Nanomedicine* (2005) **1**, 326
111. Stober, W., *et al.*, *J. Colloids Interface Sci.* (1968) **26**, 62
112. Duff, D. G., *et al.*, *Langmuir* (1993) **9**, 2301
113. Brongersma, M. L., *Nat. Mater.* (2003) **2**, 296
114. Gans, R., *Ann. Phys.* (1915) **47**, 270
115. Maali, A., *et al.*, *Physica E* (2003) **17**, 559
116. Herbst, R. S., and Shin, D. M., *Cancer* (2002) **94**, 1593
117. Wang, H., *et al.*, *Proc. Natl. Acad. Sci. USA* (2005) **102**, 15752
118. Dvorak, H. F., *et al.*, *Am. J. Pathol.* (1988) **133**, 95
119. Ishida, O., *et al.*, *Int. J. Pharm.* (1999) **190**, 49
120. Maeda, H., *Adv. Enzyme Regulation* (2001) **41**, 189
121. http://www.cytimmune.com/go.cfm?do=Page.View&pid=17
122. Portney, N., and Ozkan, M., *Anal. Bioanal. Chem.* (2006) **384**, 620
123. O'Neal, D. P., *et al.*, *Cancer Lett.* (2004) **209**, 171
124. Wong, S. F., *Clin. Ther.* (2005) **27**, 684
125. Vokes, E. E., and Chu, E., *Oncology* (2006) **20** (Supplement 2), 15
126. Litzinger, D. C., *et al.*, *Biochim. Biophys. Acta.-Biomembranes* (1994) **1190**, 99
127. Yuan, F., *et al.*, *Cancer Res.* (1994) **54**, 3352
128. Hobbs, S. K., *et al.*, *Proc. Natl. Acad. Sci. USA* (1998) **95**, 4607